Journal of Solid State Chemistry 184 (2011) 2972–2977

Contents lists available at SciVerse ScienceDirect

Journal of Solid State Chemistry

journal homepage: www.elsevier.com/locate/jssc

Synthesis, structure and conductivity of sulfate and phosphate doped $SrCoO_3$

C.A. Hancock [a], R.C.T. Slade [b], J.R. Varcoe [b], P.R. Slater [a,*]

[a] School of Chemistry, University of Birmingham, Birmingham B15 2TT, UK
[b] Chemical Sciences, University of Surrey, Guildford, Surrey GU2 7XH, UK

ARTICLE INFO

Article history:
Received 16 June 2011
Received in revised form
16 August 2011
Accepted 30 August 2011
Available online 14 September 2011

Keywords:
Solid oxide fuel cell
Cathode
Perovskite
Phosphate
Sulfate

ABSTRACT

In this paper we report the successful incorporation of sulfate and phosphate into $SrCoO_3$ leading to a change from a 2H- to a 3C-perovskite polymorph. Structural characterization by neutron diffraction showed extra weak peaks related to oxygen vacancy ordering, and these could be indexed on an expanded tetragonal cell, containing two inequivalent Co sites, similar to previously reported for Sb doped $SrCoO_3$. Conductivity measurements on the doped systems showed a large enhancement compared to the undoped hexagonal system, consistent with corner-sharing of CoO_6 octahedra for the former. Further work on the doped samples shows, however, that they are metastable, transforming back to the hexagonal cell on annealing at intermediate temperatures. The incorporation of Fe was shown, however, to improve the stability at intermediate temperatures, and these co-doped phases also showed high conductivities.

1. Introduction

Solid oxide fuel cells (SOFCs) have attracted considerable interest as an energy generation technology due to their high efficiencies and accompanying low greenhouse gas emissions. For the cathodes of SOFCs, research into new materials has been dominated by materials based on the perovskite structure, due to their generally high electronic conductivities and catalytic activity [1–3]. Traditional doping strategies for such materials have involved the partial substitution of aliovalent cations with similar size, e.g. Sr doping for La in $LaMnO_3$. Recently we have proposed an alternative doping strategy for perovskite systems with potential applications in SOFCs, namely the introduction of oxyanions (e.g. phosphate, sulfate). This work was inspired by prior work on cuprate perovskites, related to high temperature superconductors, which showed that the perovskite structure could incorporate significant levels of oxyanions (carbonate, nitrate, sulfate, phosphate) [4–21]. In order to investigate the potential of SOFC related materials to accommodate such oxyanions, we initially investigated doping into the ionic conductor $Ba_2In_2O_5$. This work showed that phosphate and sulfate could be introduced into $Ba_2In_2O_5$, leading to a structural change from brownmillerite, containing ordered oxide ion vacancies, to a cubic perovskite, where the oxide ion vacancies are disordered [22,23]. As a result of the higher symmetry, an increase in the ionic conductivity below 800 °C was observed. In addition an improvement in the stability of the compounds towards CO_2 containing atmospheres was observed [24]. In this paper we extend this work to materials with potential as electrode materials, investigating incorporation of phosphate and sulfate into $SrCoO_{3-y}$. The $SrCoO_{3-y}$ system has attracted significant interest as a promising SOFC cathode material. However, at temperatures below 900 °C the undoped phase adopts a hexagonal perovskite polymorph with low conductivity [25–27]. Detailed structural studies have indicated that this hexagonal phase is Co deficient, composition $Sr_6Co_5O_{15}$, containing face sharing of CoO_6 octahedra, similar to that of 2H-$BaNiO_3$ [27]. The formation of a hexagonal perovskite can be related to the high (>1.0) tolerance factor for undoped $SrCoO_{3-y}$. Doping $SrCoO_{3-y}$ on the Co site with a range of cations, e.g. Nb, Sb, Si has been shown to alter the stacking arrangement of the close packed oxygen layers from purely hexagonal to purely cubic (referred to as 2H and 3C, respectively). The consequent change from face-shared to corner linked CoO_6 octahedra, leads to a substantial enhancement in the electronic conductivity [28–32]. This stabilization of the 3C-perovskite framework on Nb, Sb, Si doping can be attributed to a partial reduction of Co^{4+} to Co^{3+}, thus increasing the perovskite B cation size, and hence reducing the tolerance factor. In this paper, we examine the effect of phosphate and sulfate doping on the stabilization of the 3C-perovskite polymorph.

2. Experimental

High purity $SrCO_3$, Co_3O_4, and $NH_4H_2PO_4$, and $(NH_4)_2SO_4$ were used to prepare $SrCo_{1-x}(S/P)_xO_{3-y}$ samples (considering the incorporation as PO_4^{3-}/SO_4^{2-} the formula could also be written as $SrCo_{1-x}(PO_4/SO_4)_xO_{3-4x-y}$). For the subsequently prepared Fe doped

* Corresponding author.
E-mail address: p.r.slater@bham.ac.uk (P.R. Slater).

0022-4596/$ - see front matter © 2011 Elsevier Inc. All rights reserved.
doi:10.1016/j.jssc.2011.08.040

samples, Fe_2O_3 was used as the Fe source. The powders were intimately ground (agate mortar and pestle) and heated initially to 1100 °C for 12 h. They were then ball-milled (350 rpm for 1 h, Fritsch Pulverisette 7 Planetary Mill, zirconia balls and container) and reheated to 1200 °C for a further 12 h. Powder X-ray diffraction (Bruker D8 diffractometer with Cu $K\alpha_1$ radiation) was used to demonstrate phase purity. In order to obtain further details regarding the structures of these doped phases, neutron diffraction data were collected on the HRPT diffractometer at SINQ (Paul Scherrer Institute, Villigen, Switzerland). For these samples, the as-prepared powders were furnace cooled to 350 °C and then held at this temperature for 12 h to ensure full oxygenation and hence allow a direct comparison with the conductivity data. Structure refinement made use of the GSAS suite of programs [33,34].

Pellets for conductivity measurements were prepared as follows: the pure powders, synthesized above, were first ball–milled (350 rpm for 1 h, Fritsch Pulverisette 7 Planetary Mill, zirconia balls and container), before pressing as pellets (1.3 cm diameter) and sintering at 1100 °C for 10 h. Four Pt electrodes were attached with Pt paste, and the pellet fired to 1000 °C in air for 1 h to ensure bonding to the pellet. The pellets were then furnace cooled to 350 °C and then held at this temperature for 12 h to ensure full oxygenation. The Pt electrodes were attached to 4 Pt wires in an alumina measurement jig, which was then placed in a Carbolite VST 12 furnace. Electronic conductivities were then measured using the 4 probe d.c. method (Thurlby Thandar instruments current source (TT PL310), and digital multimeter (TT 1604)).

3. Results and discussion

3.1. X-ray diffraction data

The X-ray diffraction data showed that without any phosphate doping ($x=0$), the sample was a hexagonal perovskite, $Sr_6Co_5O_{15}$, plus small concentrations of Co_3O_4 oxide impurities, as previously reported [27]. On the incorporation of a small amount of phosphate ($x=0.03$), the 3C-perovskite phase was obtained, and single phase samples could be achieved for $x \leq 0.07$ (Fig. 1). For higher phosphate levels, small concentrations of $Sr_{10}(PO_4)_6(OH)_2$ impurities were observed. Similar results were observed for sulfate doping, with an initial stabilization of the 3C-phase for low

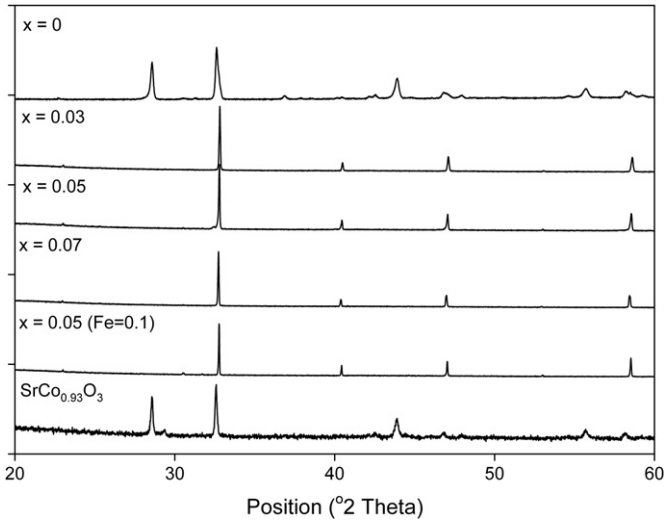

Fig. 1. Powder X-ray diffraction profiles for $SrCo_{1-x}P_xO_{3-y}$. Also included is the X-ray diffraction profile for a Co deficient sample with no added phosphate ($SrCo_{0.93}O_{3-y}$), showing that, without phosphate doping, the hexagonal polymorph is obtained even for such Co deficient samples.

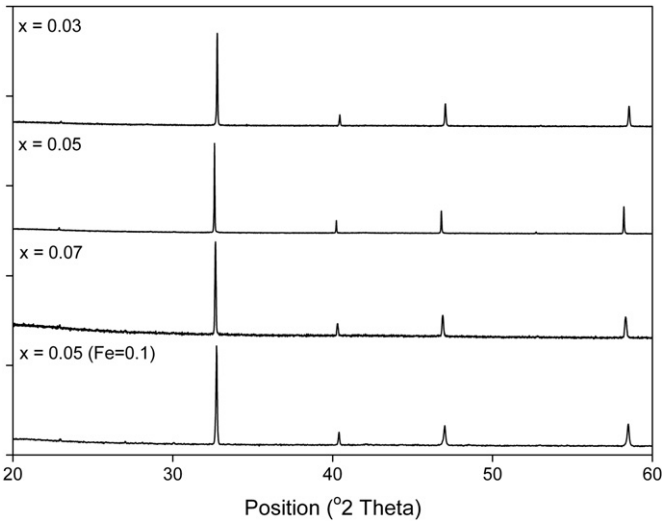

Fig. 2. Powder X-ray diffraction profiles for $SrCo_{1-x}S_xO_{3-y}$.

doping levels ($x=0.03$), and a maximum substitution limit of $x=0.07$ (Fig. 2). Confirmation of the importance of phosphate/sulfate was shown by the fact that equivalent Co deficient samples $SrCo_{1-x}O_{3-y}$ with no added sulfate/phosphate gave the hexagonal polymorph (Fig. 1).

This stabilization of the 3C-perovskite structure can be attributed to partial reduction of Co^{4+} to Co^{3+}, similar to observed for Sb, Nb doped $SrCoO_{3-x}$ [28–31]. There are two driving forces for the partial reduction in the Co oxidation state:

1. Co^{4+} is being partially replaced by higher valent P^{5+}/S^{6+}.
2. The introduction of P/S on the perovskite B cation site requires the creation of oxygen vacancies to convert the coordination to tetrahedral (as required for PO_4^{3-}/SO_4^{2-}), which in turn leads to a requirement for partial reduction of Co.

To describe these effects we can write the following defect equations for PO_4^{3-}/SO_4^{2-} incorporation:

$$NH_4H_2PO_4 + 4Co_{Co} + O_O \rightarrow P^{\bullet}_{Co} + 3Co_{Co}' + V_O^{\bullet\bullet} + {}^3/_4O_2 + NH_3 + {}^3/_2H_2O + CoO_2 \quad (1)$$

$$(NH_4)_2SO_4 + 5Co_{Co} + O_O \rightarrow S^{\bullet\bullet}_{Co} + 4Co_{Co}' + V_O^{\bullet\bullet} + O_2 + 2NH_3 + H_2O + CoO_2 \quad (2)$$

As can be seen from Eqs. (1) and (2), the introduction of phosphate and sulfate groups will lead to significant reduction of the Co oxidation state. The stabilization of the 3C-perovskite polymorph on sulfate and phosphate doping can then be related to the increased Co^{3+} level, and hence average B cation size, reducing the tolerance factor. It is also possible that the presence of PO_4^{3-}/SO_4^{2-} units may help to disfavor the presence of face sharing, thus promoting corner sharing and hence the formation of the 3C-perovskite.

3.2. Electronic conductivity data

Following the observation of the formation of a 3C-perovskite structure on sulfate/phosphate doping, the conductivities of these phases were then analyzed. These data showed a significant enhancement in the conductivity (Table 1, Figs. 3 and 4), consistent with a change from a 2H-polymorph with face sharing of octahedra, to a 3C-polymorph with corner sharing. For the phosphate doped samples, the highest conductivity was observed for $x=0.05$, while

Table 1
Conductivities (S cm^{-1}) for $SrCo_{1-x}Z_xO_{3-y}$ (Z=P, S) at room temperature and 600 °C.

Nominal Composition	Phosphate doped		Sulfate doped	
	25 °C	600 °C	25 °C	600 °C
$SrCoO_{3-y}$	1.7	6.7	1.7	6.7
$SrCo_{0.97}Z_{0.03}O_{3-y}$	204	100	189	120
$SrCo_{0.95}Z_{0.05}O_{3-y}$	323	128	58	25
$SrCo_{0.93}Z_{0.07}O_{3-y}$	67	29	66	42
$SrCo_{0.85}Fe_{0.1}Z_{0.05}O_{3-y}$	125	63	36	71

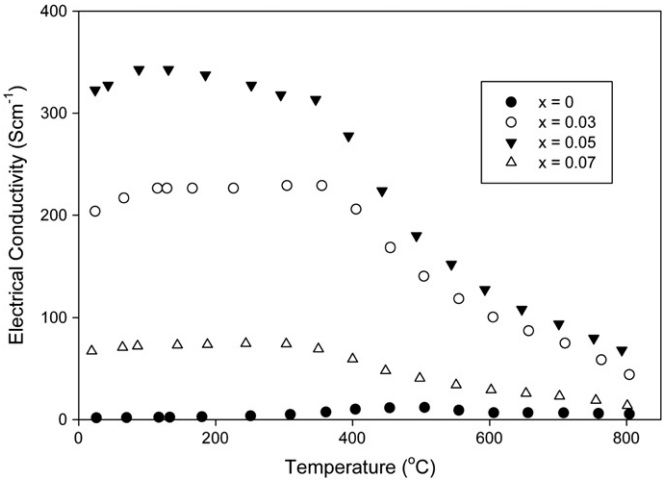

Fig. 3. Temperature dependence of the electronic conductivity for $SrCo_{1-x}P_xO_{3-y}$.

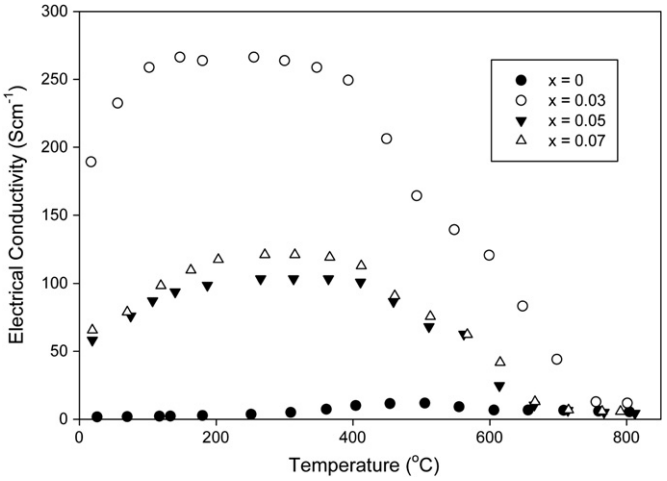

Fig. 4. Temperature dependence of the electronic conductivity data for $SrCo_{1-x}S_xO_{3-y}$.

for sulfate doping the highest conductivity was for x=0.03. While S, P doping enhances the electronic conductivity by stabilising the 3C-perovskite, it will also have a negative effect in terms of partially disrupting the Co–O network. Hence for S doping, the highest conductivity is observed for the lowest S dopant level that stabilises the 3C-perovskite. In contrast, for P doping, the higher conductivity was observed for x=0.05 compared to x=0.03.

While these initial conductivity results showed very high values, further work on thermal cycling of the sample resulted in a gradual reduction in conductivity. Furthermore, annealing the samples overnight at intermediate temperatures (≈ 750 °C) led to a large decrease in conductivity, with X-ray diffraction indicating

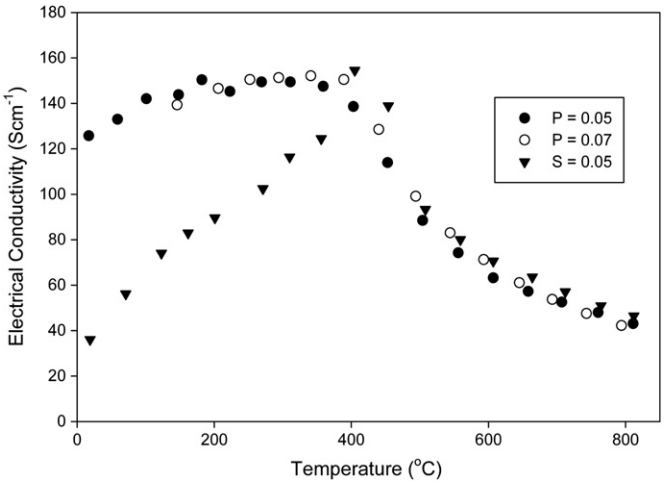

Fig. 5. Temperature dependence of the electronic conductivity data for $SrCo_{0.9-x}Fe_{0.1}(P/S)_xO_{3-y}$.

the conversion to the hexagonal perovskite. Thus it would appear as if the doped phases are metastable, and so the lower conductivity on phosphate doping for the x=0.03 compared to the x=0.05 sample may be related to the presence of local regions of hexagonal symmetry. Similar results demonstrating metastability of the 3C-perovskite structure have been shown in a number of other studies on $SrCoO_3$ and related systems [35,36].

In order to try to improve the thermodynamic stability of these oxyanion doped phases, co-doping with Fe was examined. This work showed that the additional incorporation of 10 mol% Fe in place of Co helped to stabilize the 3C-perovskite phase, with phases with compositions $SrCo_{0.85}Fe_{0.1}(P/S)_{0.05}O_{3-y}$ showing good stability (no observed changes in X-ray diffraction pattern on annealing overnight at 750 °C), with high conductivities still observed (Table 1, Fig. 5).

The conductivities for all samples show a decrease above ≈ 350 °C, which can be attributed to oxygen loss above this temperature, as observed in related studies on doping $SrCoO_3$ with similar size cations (Nb, Sb) [28–31].

3.3. Neutron diffraction structural study of phosphate doped samples

The structures of three phosphate doped samples, $SrCo_{1-x}P_xO_{3-y}$ (x=0.03, 0.07) and $SrCo_{0.83}Fe_{0.1}P_{0.07}O_{3-y}$, were examined using neutron diffraction. The neutron diffraction data showed the presence of extra peaks not apparent in the X-ray diffraction data, and their intensity reduced with increasing phosphate content. These extra peaks were indexed to an expanded tetragonal *P4/mmm* cell (Fig. 6), which has been correlated to a degree of oxygen vacancy ordering, as seen previously for related studies on Sb doping [31]. This leads to preferential accommodation of the oxide ion vacancies in the O2, and O3 sites surrounding the Co2 site, along with a preferential occupation of this site by P.

The final refined structural data are given in Tables 2, 4, and 6 with selected bond distances in Tables 3, 5, and 7. The observed, calculated, and difference profiles are given in Figs. 7–9. In these refinements the atomic displacement parameters for the oxygen sites were constrained to be equal, as were the parameters for the Co sites. The final refined values for the P content are in good agreement with those expected from the starting composition. For the Fe doped sample, $SrCo_{0.83}Fe_{0.1}P_{0.07}O_{3-y}$, it was not possible to refine independent Co, Fe, P occupancies due to the presence of too many variables. Consequently the P content was fixed at that expected and assumed to be located on the Co2 site,

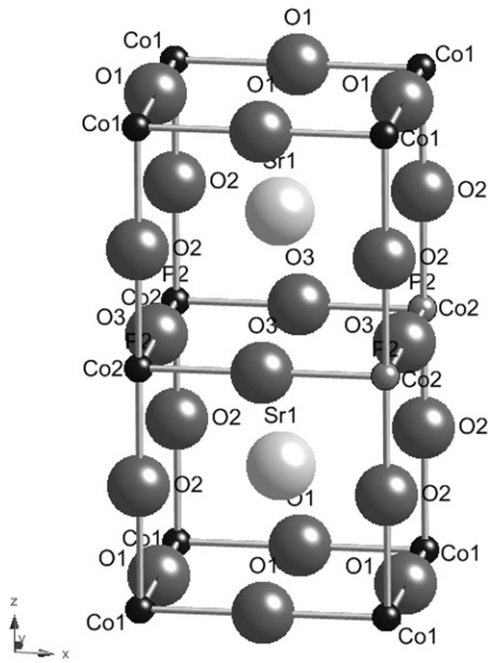

Fig. 6. Structure of oxyanion doped $SrCoO_{3-y}$ showing the presence of two Co sites: the P, S (from the phosphate, sulfate groups) preferentially substitute at the Co2 site.

Table 2
Structural parameters for $SrCo_{0.97}P_{0.03}O_{3-y}$.

Atom	x	y	z	100Uiso	Occupancy
Co1	0	0	0	1.28 (4)	1
Co2	0	0	0.5	1.28 (4)	0.94 (3)
Sr1	0.5	0.5	0.2354 (2)	1.19 (3)	1
O1	0.5	0	0	2.54 (2)	1
O2	0	0	0.2547 (3)	2.54 (2)	0.83 (2)
O3	0.5	0	0.5	2.54 (2)	0.79 (1)
P2	0	0	0.5	1.28 (4)	0.06 (3)

Space group *P*4/*mmm*, $a=3.86123(9)$ Å, $c=7.7330(5)$ Å, $\chi^2=7.063$, Rwp=3.8%.

Table 3
Bond distances for $SrCo_{0.97}P_{0.03}O_{3-y}$.

Bond	Bond length (Å)
Co1–O1 (x4)	1.93061 (4)
Co1–O2 (x2)	1.9695 (27)
Co2/P2–O2 (x2)	1.8970 (27)
Co2/P2–O3 (x4)	1.93061 (4)
Sr1–O1 (x4)	2.6535 (11)
Sr1–O2 (x4)	2.73437 (15)
Sr1–O3 (x4)	2.8132 (12)

Table 4
Structural parameters for $SrCo_{0.93}P_{0.07}O_{3-y}$.

Atom	x	y	z	100Uiso	Occupancy
Co1	0	0	0	1.49 (3)	1
Co2	0	0	0.5	1.49 (3)	0.83 (2)
Sr1	0.5	0.5	0.2420 (3)	1.51 (2)	1
O1	0.5	0	0	2.44 (2)	1
O2	0	0	0.2539 (5)	2.44 (2)	0.77 (1)
O3	0.5	0	0.5	2.44 (2)	0.80 (1)
P2	0	0	0.5	1.49 (3)	0.17 (2)

Space group *P*4/*mmm*, $a=3.8680(1)$ Å, $c=7.7393(7)$ Å, $\chi^2=4.354$, Rwp=2.87%.

Table 5
Bond distances for $SrCo_{0.93}P_{0.07}O_{3-y}$.

Bond	Bond length (Å)
Co1–O1 (x4)	1.93402 (7)
Co1–O2 (x2)	1.965 (4)
Co2/P2–O2 (x2)	1.904 (4)
Co2/P2–O3 (x4)	1.93402 (7)
Sr1–O1 (x4)	2.6922 (15)
Sr1–O2 (x4)	2.73669 (16)
Sr1–O3 (x4)	2.7798 (15)

Table 6
Structural parameters for $SrCo_{0.83}Fe_{0.1}P_{0.07}O_{3-y}$.

Atom	x	y	z	100Uiso	Occupancy
Co1	0	0	0	1.04 (4)	0.90 (1)
Co2	0	0	0.5	1.04 (4)	0.82 (1)
Sr1	0.5	0.5	0.2446 (4)	1.60 (2)	1
O1	0.5	0	0	2.26 (2)	1
O2	0	0	0.2533 (8)	2.26 (2)	0.69 (1)
O3	0.5	0	0.5	2.26 (2)	0.82 (1)
Fe1	0	0	0	1.04 (4)	0.10 (1)
Fe2	0	0	0.5	1.04 (4)	0.04 (1)
P2	0	0	0.5	1.04 (4)	0.14

Space group *P*4/*mmm*, $a=3.8675(1)$ Å, $c=7.7411(5)$ Å, $\chi^2=3.362$, Rwp=3.12%.

Table 7
Bond distances for $SrCo_{0.83}Fe_{0.1}P_{0.07}O_{3-y}$.

Bond	Bond length (Å)
Co1/Fe1–O1 (x4)	1.93377 (5)
Co1/Fe1–O2 (x2)	1.961 (6)
Co2/P2/Fe2–O2 (x2)	1.909 (6)
Co2/P2/Fe2–O3 (x4)	1.93377 (5)
Sr1–O1 (x4)	2.7067 (21)
Sr1–O2 (x4)	2.73559 (15)
Sr1–O3 (x4)	2.7653 (22)

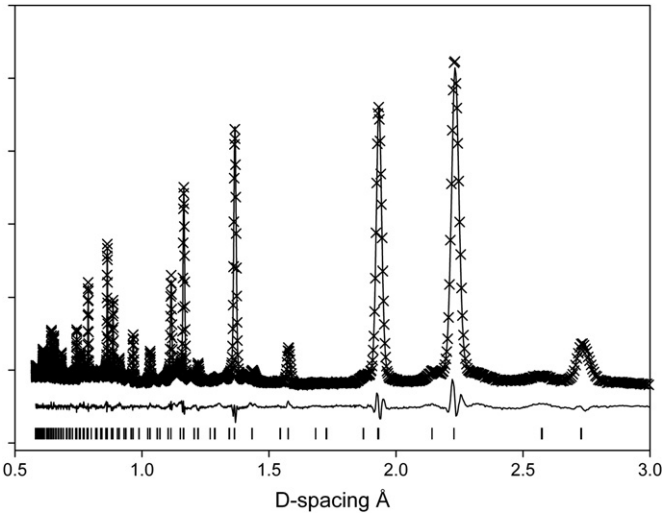

Fig. 7. Observed, calculated and difference neutron diffraction profiles for $SrCo_{0.97}P_{0.03}O_{3-y}$.

as observed for the $SrCo_{1-x}P_xO_{3-y}$ samples. The Fe/Co content across each site was then varied.

The expanded tetragonal cell leads to two Co sites (Fig. 6), with a preference for the location of the P (from the phosphate groups)

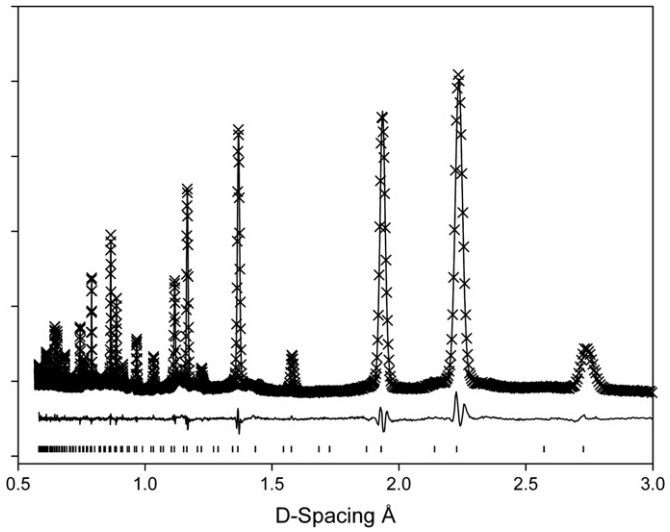

Fig. 8. Observed, calculated and difference neutron diffraction profiles for $SrCo_{0.93}P_{0.07}O_{3-y}$.

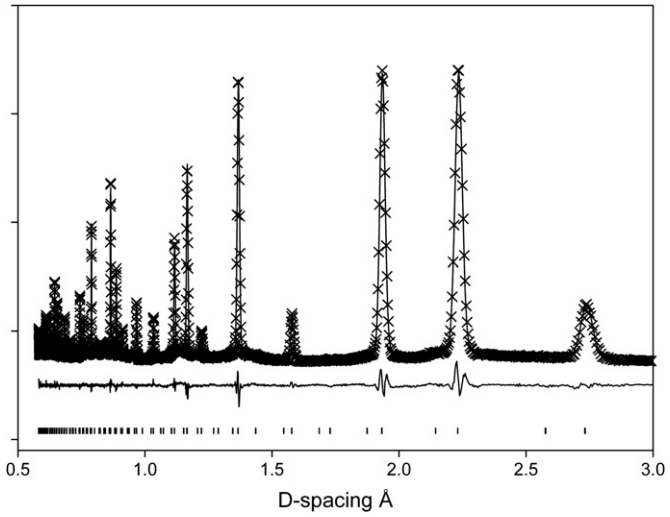

Fig. 9. Observed, calculated and difference neutron diffraction profiles for $SrCo_{0.83}Fe_{0.1}P_{0.07}O_{3-y}$.

at the Co2 site, which has oxide ion vacancies around it. For the Fe doped samples, the refinement indicates a small preference for Fe in the Co1 site. The two Co sites show different bond lengths, with the $(Co1)O_6$ octahedra showing slightly longer apical bond lengths, while for the $(Co2)O_6$ octahedra, the apical bond lengths are shorter. The distortions are, however, much smaller than previously observed for Sb doped $SrCoO_{3-x}$, where much larger bond length differences were observed between the two Co sites (maximum difference in the present study = 0.07 Å, compared to 0.3 Å for Sb doped $SrCoO_{3-x}$)[31]. Moreover, in this study, the shorter apical bond lengths are to the Co2 site rather than the Co1 site, which may be related to the smaller dopant in the present study. The oxide ion vacancies are preferentially located in the O2 and O3 sites surrounding the Co2/P2 site. High atomic displacement parameters were observed for the oxide ion sites, as previously observed for Sb doped $SrCoO_{3-x}$, which in the latter has been attributed to dynamical tilting of the octahedral [31]. In the present systems, a further contribution to these high values will be due to local distortions caused by the presence of sulfate and phosphate groups. In particular, the oxide ions for these oxyanions will be significantly displaced from the ideal oxide ion sites in the structure to achieve the required tetrahedral geometry for phosphate. However, it was not possible to refine separate positions for these oxide ion sites, due to the low levels and the likely variation in orientation, as seen in other studies of oxyanion containing perovskites [6,21].

4. Conclusions

In this work, phosphate and sulfate were successfully incorporated into the perovskite structure of $SrCoO_{3-y}$ leading to an enhancement of the electronic conductivity, attributed to a change from a 2H- to a 3C-perovskite. The 3C-perovskite was, however, shown to be metastable and converted back to the hexagonal perovskite on annealing at intermediate temperatures ($\approx 750\ ^{\circ}C$). The thermodynamic stability was improved by co-doping with Fe, with high conductivity maintained, suggesting that these co-doped systems may have potential as SOFC cathode materials.

Acknowledgments

We would like to express thanks to the EPSRC for funding (Grant EP/G009929/2—studentship for CAH). The Bruker D8 diffractometer used in this research were obtained through the Science City Advanced Materials project: Creating and Characterising Next generation Advanced Materials project, with support from Advantage West Midlands (AWM) and part funded by the European Regional Development Fund (ERDF). We would like to thank SINQ for neutron diffraction time and Vladimir Pomjakushin for help with the neutron diffraction experiments.

References

[1] A. Orera, P.R. Slater, Chem. Mater. 22 (2010) 675.
[2] A.J. Jacobson, Chem. Mater. 22 (2010) 660.
[3] A. Lastaberg, S.J. Skinner, J. Mater. Chem. 16 (2006) 3161.
[4] C. Greaves, P.R. Slater, J. Mater. Chem. 1 (1991) 17.
[5] C. Greaves, P.R. Slater, Physica C 175 (1991) 172.
[6] P.R. Slater, C. Greaves, M. Slaski, C.M. Muirhead, Physica C 208 (1993) 193.
[7] Y. Miyazaki, H. Yamane, N. Ohnishi, T. Kajitani, K. Hiraga, Y. Morii, S. Funahashi, T. Hirai, Physica C 198 (1992) 7.
[8] A. Maignan, M. Hervieu, C. Michel, B. Raveau, Physica C 208 (1993) 116.
[9] K. Kinochita, T. Yamada, Nature 357 (1992) 313.
[10] B. Raveau, M. Hervieu, D. Pelloquin, C. Michel, R. Retoux, Z. Anorg. Allg. Chem. 631 (2005) 1831.
[11] D. Pelloquin, M. Hervieu, C. Michel, N. Nguyen, B. Raveau, J. Solid State Chem. 134 (1997) 395.
[12] J.C.G. Gonzalez, J.A. Aguiar, S. Quezado, L.M. Dezanetie, C.W. Chu, A.B. Dominguez, Physica C 354 (2001) 441.
[13] K.N. Marimuthu, U.V. Varadaraju, M. Hervieu, B. Raveau, S.K. Malik, W.B. Yelon, J. Solid State Chem. 150 (2000) 188.
[14] M. Isobe, Y. Matsui, E. Takayama-Muromachi, Physica C 273 (1996) 72.
[15] Y. Laureiro, E. Moran, R. Rojas, M.A. Alario-Franco, J. Mater. Chem. 6 (1996) 1517.
[16] E. Takayama-Muromachi, Y. Matsui, J. Ramirez-Castellanos, Physica C 252 (1995) 221.
[17] P.R. Slater, C. Greaves, M. Slaski, Physica C 235 (1994) 741.
[18] C. Greaves, M. Al Mamouri, P.R. Slater, P.P. Edwards, Physica C 235 (1994) 158.
[19] R. Nagarajan, S. Ayyappan, C.N.R. Rao, Physica C 220 (1994) 373.
[20] S. Ayyappan, V. Manivannan, G.N. Subbana, C.N.R. Rao, Solid State Commun. 87 (1993) 551.
[21] P.R. Slater, C. Greaves, Physica C 223 (1994) 37.
[22] J.F. Shin, L. Hussey, A. Orera, P.R. Slater, Chem. Commun. 46 (2010) 4613.
[23] J.F. Shin, A. Orera, D.C. Apperley, P.R. Slater, J. Mater. Chem. 21 (2011) 874.
[24] J.F. Shin, P.R. Slater, J. Power Sour. 196 (2011) 8539.
[25] J.-C. Grenier, S. Ghodbane, G. Demazeau, Mater. Res. Bull. 14 (1979) 831.
[26] P.D. Battle, T.C. Gibb, A.T. Steel, Dalton Trans. (1988) 83.
[27] W. Harrison, S.L. Hedwood, A.J. Jacobson, Chem. Commun. 1953 (1995).
[28] A. Aguadero, C. de la Calle, J.A. Alonso, M.J. Escudero, M.T. Fernandez–Diaz, L. Daza, Chem. Mater. 19 (2007) 6437.

[29] A. Aguadero, D. Perez–Coll, C. de la Calle, J.A. Alonso, M.J. Escudero, L. Daza, J. Power Sour. 192 (2009) 132.
[30] K. Zhang, R. Ran, L. Ge, Z.P. Shao, W.Q. Jin, N.P. Xue, J. Membr. Sci. 323 (2008) 436.
[31] A. Aguadero, J.A. Alonso, D. Perez–Coll, C. de la Calle, M.T. Fernandez–Diaz, J.B. Goodenough, Chem. Mater. 22 (2010) 789.
[32] C.A. Hancock, P.R. Slater, Dalton Trans. 40 (2011) 5599.
[33] A.C. Larson, R.B. Von Dreele, Los Alamos National Laboratory, Report No LAUR 96–748, 2000.
[34] B.H. Toby, J. Appl. Cryst. 34 (2001) 210.
[35] T. Nagai, W. Ito, T. Sakon, Solid State Ionics 177 (2007) 3433.
[36] S. Svarcova, K. Wiik, J. Tolchard, H.J.M. Bouwmeester, T. Grande, Solid State Ionics 178 (2008) 1787.